
Article:
Fowler, A.C., Kember, G.C. and Ng, F. orcid.org/0000-0001-6352-0351 (2025) Towards a theory for the formation of sea stacks. Proceedings of the Royal Society A: Mathematical, Physical and Engineering Sciences, 481 (2328). 20250332. ISSN: 1364-5021

https://doi.org/10.1098/rspa.2025.0332

PROCEEDINGS A

royalsocietypublishing.org/journal/rspa

Research

Cite this article: Fowler AC, Kember GC, Ng FSL. 2025 Towards a theory for the formation of sea stacks. *Proc. R. Soc. A* **481**: 20250332. https://doi.org/10.1098/rspa.2025.0332

Received: 15 April 2025
Accepted: 13 October 2025

Subject Areas:
geophysics, applied mathematics

Keywords:
sea stacks, erosion, instability, coastal geomorphology

Author for correspondence:
A. C. Fowler
e-mail: andrew.fowler@ul.ie

Electronic supplementary material is available online at https://doi.org/10.6084/m9.figshare.c.8116001.

THE ROYAL SOCIETY PUBLISHING

Towards a theory for the formation of sea stacks

A. C. Fowler[1,2], G. C. Kember[3] and F. S. L. Ng[4]

[1]MACSI, University of Limerick, Limerick, Ireland
[2]OCIAM, University of Oxford, Oxford, UK
[3]Department of Engineering Mathematics, Dalhousie University, Halifax, Nova Scotia, Canada
[4]School of Geography and Planning, University of Sheffield, Sheffield, UK

ACF, 0000-0002-2062-6372; FSLN, 0000-0001-6352-0351

We provide a continuum model that has the capability to explain the dynamical processes which lead to the formation of sea stacks. The basic concept is that a uniformly retreating sea cliff face can be unstable to the formation of spatial undulations, initially as sine waves, but with increasing contortion as the sinuosity develops. The mechanism for instability is the positive feedback created by enhanced erosion rate caused by the shore debris created by cliff collapse. This mechanism is somewhat similar to the morphological effects of wave-induced sand transport in forming irregular beach-bounded coastlines. The key ingredient of the theory which can potentially enable cave formation and isolated stacks to occur is that the relevant spatial variable describing along-shore transport is the along-shore arc length. We formulate the model, show that it provides the sought-for instability, and give numerical solutions for the resulting shore-line. As yet, we have not found self-intersecting shore-lines, which would be the harbinger of sea stack formation.

1. Introduction

Sea stacks are small islands with cliff faces which are found close to a shore-line of coastal cliffs. There are many examples around the world (see for example [1, pp. 515 ff], [2, pp. 271 ff] or [3, pp. 90 ff]), including for example the stacks of Duncansby in northern Scotland, the Old Man of Hoy in the Orkney Islands, the Twelve Apostles of the Port Campbell coast of Victoria,

Figure 1. Bishop's Island is a sea stack off the west coast of County Clare, Ireland.

Australia [4], but for this study we take our inspiration from the sea stacks which lie near the cliffs south of Kilkee on the Loop Head peninsula in West Clare, Ireland. A famous example of one such sea stack is the Bishop's Island (figure 1), so called because it contains the ruins of a small monastic settlement from early Christian times [5, p. 146], and we might suppose these date from at least a thousand years ago, when presumably the island was joined to the mainland; it is now 100 m offshore. The question we wish to address here is, what is the physical mechanism whereby these stacks form?

One straightforward suggestion (and this is probably geomorphological orthodoxy) is that they form due to a process of differential erosion, such as causes the formation of volcanic plugs [1, p. 191]. However, this kind of process may not always work in sedimentary rocks, such as those on the Loop Head peninsula, which consist of Carboniferous shales and sandstones [6] which are sub-horizontally bedded (and not vertically, as in the case of volcanic plugs). Nor is it easy to fathom why rocks deposited as turbidites or debris fans should have a cylindrical structure, unless deposited in lakes—but very small lakes. Regular folding of the strata or sub-vertical jointing [7,8] can provide weak rock which is subject to cave or inlet formation. Extension of caves through headlands forms arches, and the collapse of the overlying bridge produces the stack, and this qualitative view has been expressed for sea arches and stacks by Shepard & Kuhn [9].

The above view associates irregularity in cliff shore-line erosion with irregularity in the substrate. In this paper, we want to take an orthogonal viewpoint, and ask the question, can the process of erosion *in itself* promote the development of irregular coastlines, and in particular, can we develop a mathematical model which will predict the formation of sea stacks, *even in the absence of promotional joints and faults*? In this view, the occurrence of weak zones provides an initial perturbation, but it is the dynamics of erosion which can cause their further evolution.

In a wider geomorphological context, we can relate the aims of the present study to that of other geomorphological features. Drumlins [10], river meanders [11], fluvial and aeolian dunes [12] and ice sails [13] are all examples of bedforms which are thought to form through an instability mechanism. An interesting example in the present context is that of glacial flutes. These are subglacial ridges, of the order of a metre wide and high, and hundreds of metres long, aligned with the (former) ice flow, and exposed as the glacier retreats. Often, but not always, they have

a lodged boulder at their head [14], which would thus seem to provide the natural explanation for their formation. But boulders are not always present, and indeed flutes seem to have a spatial regularity [15], which suggests an instability mechanism. Boulton [16] was quite against the idea of a spatial instability, but Gordon *et al.* [17] and others since are less sure. The analogy with stack formation is clear: differential erosion *might* cause *some* stacks, but unless it causes *all*, it seems an instability mechanism is also necessary, and differential erosion then becomes an agent and not a cause.

There is an extensive literature on the description and modelling of rocky coasts, and reviews have been provided by Naylor *et al.* [18], Trenhaile [19] and Trenhaile [20]. In particular, Naylor *et al.* comment on the lack of treatments of stack formation. The models come in a variety of forms [21,22], and some are cellular models [23–25], while some use named codes (SCAPE, NEWTS) [23,26]. The principal proponent of partial differential equation models for shore-line evolution has been Brad Murray and his co-workers (e.g. [27–31]), and the model we develop here takes its inspiration from this literature, although with some detailed but significant differences.

Much of the interest has been on retreat rates and cross-shore profiles (e.g. [22–24,32]), or on the effects of tectonic uplift and sea-level rise [21,26], but there has also been interest in the shore-line effects of along-shore differential erosion [20,25,30,31]. Despite all this activity, models for the planform evolution of rocky coast profiles are not well developed. In contrast to subjects such as dune formation (e.g. [33]) or river channel morphology (e.g. [34]), their formulation in terms of partial differential equations is not yet mature.

The erosion models of Murray and his co-workers involve cliff erosion in the presence of sandy beaches. Particularly for sandy cliffs, it has long been known that the presence of beaches affects the rate of cliff recession [19,35,36]; in particular, on the basis of laboratory experiments, Sunamura [37] makes the important point that the effects of beach extent have a non-monotonic effect on cliff erosion rates: small beaches allow for an increasing effect on erosion, owing to the abrasive properties of sand-laden water waves, whereas extensive beaches protect against erosion by absorbing tidal wave energy and thus effectively armouring the cliff.

The basis of the models developed by these researchers is a combination of a prescribed onshore recession (i.e. erosion) rate, which is taken to be a function of beach width, and a mass conservation for the beach width itself, which includes an along-shore beach flux. An expression for this was given by Komar [38]; the flux depends on the incoming wave angle to the shore, and in an absolute frame of reference, this will depend on the along-shore beach angle, and thus provides a diffusive term in the beach conservation equation [39, p. 253]. We comment in more detail on this below.

Much of the interest of Ashton & Murray [28] and later Limber & Murray [29] concerns instability of a receding shore-line. The latter paper gives a coherent account of the theory.[1] Limber & Murray [40] used this model to study the formation of sea stacks. Whereas in their 2011 paper [29] they solved the partial differential equations numerically, in their 2015 paper [40] they reformulate this as a cellular numerical model, and the conclusions may be less robust as a consequence.

In this paper, we also develop a mathematical model for sea stack formation, but while it is closely related to the Limber–Murray model, it is distinctive in several respects. Specifically, the spatial variable is the along-shore arc length, and this allows for the possibility of a self-intersecting shore-line (which would be interpreted as cave and then stack formation). A milder distinction is in the choice of functional form for the removal rate of coastal sediment to the deep sea: this is essentially a choice of parameter range. The other important ingredient is a dependence of erosion rate on shore-line curvature: this is mathematically important as it provides a smoothing mechanism for 'curvature shocks' (jumps in along-shore shore-line slope); further discussion of this term can be found in §6.

We postpone further discussion of the Limber–Murray model until we present our own model in §2, so we can then relate the two models in detail. In addition, our focus here is on the

[1]Note that the sign of S in eqn. (3) in that paper appears to be incorrect.

Figure 2. Farther down the coast on the Loop Head peninsula from figure 1, near the remains of Dunlicky Castle, an inlet has been eroded from the cliffs. At its head, a tell-tale layer of eroded boulders can be seen.

mathematical properties of the solutions of the model, and whether they have the possibility of describing the evolution of sea stacks. Our approach is, therefore, somewhat orthogonal to that of Limber and Murray, whose emphasis was more on simulation.

The formation of sea stacks is, for the applied mathematician, a problem of stability. We expect an eroding cliff face to have a solution of an appropriate model in which the shore-line is straight, and we then expect this solution to be unstable in certain circumstances (but stable in others) to the formation of wave-like disturbances, and we then hope that the nonlinear evolution of these will lead to behaviour which we can interpret as cave formation and thus stack formation. The fact that stacks form on some coasts but not on others would require conditions which promote instability, and would further require that the nonlinear development of the resulting perturbations would cause shore-line self-intersection.

The instability mechanism is motivated by figure 2, which shows an eroding inlet which is in the process of forming a rather large sea stack at Dunlicky Castle on the Loop Head Peninsula.

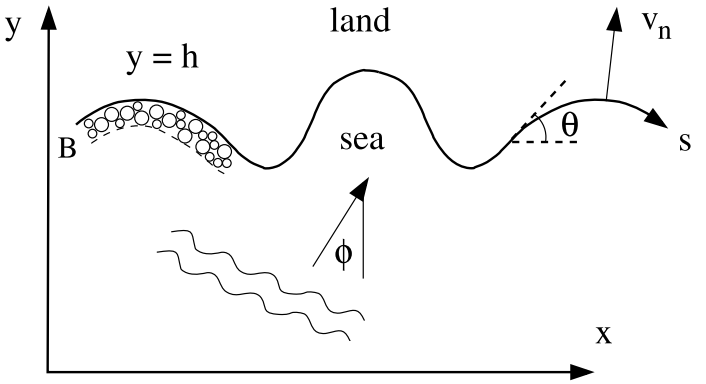

Figure 3. Geometry of cliff erosion.

The idea is that the erosion of the cliff by undercutting and collapse leads to the accumulation of boulder detritus at the foot of the cliff face, and this detritus will cause an accelerated erosion when it is activated by storms. Of course, in essence this is the same idea as the long-standing idea of beach-enhanced erosion, but is promoted here in a slightly different context. As we shall see, there are also slight variations in the way the model is proposed, which may also reflect on the earlier beach/cliff models, and we comment on these variations below.

2. Mathematical model

We consider an eroding shore-line bounded by vertical cliffs. Erosion causes the cliffs to retreat, and the supposition that the cliffs remain vertical implies that the model can be taken to be two-dimensional. The geometry of the model is shown in figure 3. In plan view, the (vertical) cliff face is at $y = h$, which is a function of along-shore distance x and time t. The sea lies in $y < h$ and the landward side is in $y > h$. We suppose that the eroded material from the cliff forms a talus slope which constitutes a boulder beach, which may be partly or wholly submerged. We suppose this is of width B, depth (at the cliff) h_b, and has a (small) slope angle β, so that

$$h_b = B \tan \beta. \tag{2.1}$$

The basic equation of the model is a prescribed erosion rate E which determines the normal velocity of the cliff face v_n,

$$v_n = \frac{h_t}{(1 + h_x^2)^{1/2}} = E, \tag{2.2}$$

where the subscripts t and x denote partial derivatives. Note that this assumes h is single-valued equation (2.2) gains a minus sign if h turns over on itself). Here E is the rate of shore-line erosion, and has units m yr^{-1}. Because the model is two-dimensional, it cannot distinguish between cliff collapse and cave formation, for which a three-dimensional generalization of the present model would be necessary.

The key idea in our model is that the erosion rate E depends on the concentration of eroded rock fragments. We take the local concentration of rock offshore (denoted as c) to be the volume of eroded rock per unit area of sea floor, thus having units of m. Let us take local orthogonal curvilinear coordinates[2] (s, η), where s is arc length along the shore-line (the positive direction of s has the land on the left), as in figure 3, and η is the distance inshore along the normal to the shore-line.

[2]Local, because the normal coordinates will intersect at some distance from the shore-line; if the sediment is concentrated close to the shore-line, this does not matter.

The sediment is subject to along-shore and onshore fluxes, which we denote as $q_\parallel$ and $q_\perp$ with units $\mathrm{m}^2\,\mathrm{s}^{-1}$, and the sediment concentration satisfies the equation (in curvilinear coordinates)

$$c_t = -\frac{1}{h_1}\left[\frac{\partial q_\parallel}{\partial s} + \frac{\partial (h_1 q_\perp)}{\partial \eta}\right], \quad h_1 = 1 - \kappa\eta, \tag{2.3}$$

in which κ is the shore-line curvature (later defined explicitly in equation (4.1)).

We assume that the bulk of the detritus occupies the beach $-B < \eta < 0$ at the base of the cliff, and then we define the shore-line sediment concentration as

$$C = \int_{-B}^{0} c\,\mathrm{d}\eta. \tag{2.4}$$

In a more general model, we would also allow for the erosive dependence on grain size, and then also include a description of comminution [41], but this is ignored in the present model.

We assume $\kappa\eta \sim \kappa B \ll 1$ on the basis that $B \ll l$, where l is a typical length scale over which the shore-line varies, so that $h_1 \approx 1$, and then integration of equation (2.3) over the shore-line detritus width B yields

$$C_t = -q_s + q_\perp|_{-B} - q_\perp|_0 \quad \text{and} \quad q = \int_{-B}^{0} q_\parallel\,\mathrm{d}\eta, \tag{2.5}$$

where the subscript t denotes partial differentiation with respect to time t, and the subscript s denotes partial differentiation with respect to arc length s along the shore-line.

The last term on the right-hand side of the equation for C is the cliff erosion rate. It seems reasonable to suppose that in an unhindered environment, this depends linearly on the total boulder concentration C, weighted by a coefficient r, but we also suppose that the erosional efficiency is reduced by the armouring effect of the concentration, thus we take

$$-q_\perp|_0 = HE = rA(C)C; \tag{2.6}$$

here H is the cliff height, so r has units yr^{-1}, and $A(C)$ is a dimensionless armouring factor, which is monotonically decreasing with C.

The second term on the right-hand side of equation (2.5) is the loss rate of detritus to the deep sea. We suppose a simple linear relationship,

$$q_\perp|_{-B} = -\lambda(C - C_0); \tag{2.7}$$

tides enable a seaward transport of excess sediment until there is a balance between shoreward advection and seaward transport. The model we thus propose for C is

$$C_t = rAC - \lambda[C - C_0] - q_s. \tag{2.8}$$

The process of sediment transport is enabled by bedload transport in the following way. Here we follow the discussion of Longuet-Higgins [42]. Incoming waves along rays at an angle of incidence ϕ to the y axis (ϕ is positive if the waves approach from the left) deliver an along-shore *radiation stress* to the water beneath which is given by (Longuet-Higgins, eqn. (34) with $\alpha = 0.4$),

$$\tau_\parallel = 0.2\rho_w g h_w \tan\beta \sin(\phi + \theta), \tag{2.9}$$

where ρ_w is the water density, h_w is the water depth, β is the slope angle of the sediment beach wedge and θ is the slope angle of the shore-line to the x axis, as indicated in figure 3 (thus $\partial h/\partial s = \sin\theta$).

Generally, one would suppose that q would be a nonlinear function of $\tau_\parallel$, e.g. $q \propto \tau_\parallel^{3/2}$, which is the Meyer-Peter & Müller [43] law, if we ignore the critical Shields stress [44]. However, we make an algebraically simpler assumption that $q \propto \tau_\parallel$. Why should we do this? There are two reasons. First, debris transport at rocky cliffs is not a continuous process and is largely enabled during severe storms. But, the Meyer-Peter/Müller and other such transport laws apply to steady experimental conditions with uniform flows. Second, Longuet-Higgins's radiation stress is computed for linear and regular wave trains, quite unlike the raging torrents which occur at

rocky cliffs during storms. While his formula provides a platform for a theoretical description, it is not necessarily the case that it is quantitatively accurate.

Next, we allow for an along-shore variation in h_b (and thus also C). The effect of such a slope is to modify the driving stress to the form (cf. [45, eqn. (2.3)])

$$\tau_e = \tau_{\parallel} - \Delta\rho\, g D_s \frac{\partial h_b}{\partial s}, \tag{2.10}$$

where $\Delta\rho$ is the difference between rock density and water density and D_s is the (boulder) grain size. In summary, we propose a sediment flux of the form (assuming a small wedge slope β)

$$q = KB\left[0.2\rho_w g h_w \tan\beta \sin(\phi+\theta) - \Delta\rho\, g D_s \frac{\partial h_b}{\partial s}\right]. \tag{2.11}$$

While the stress delivered to the bed is the same for all particles, their transport will depend on size, since the critical Shields stress depends on grain size [44]. Hence, the sediment transport coefficient K will generally depend on grain size, but this complication is ignored here, as we are omitting reference to grain size distribution. To simplify matters further, we suppose waves approach the coast normally, so that $\phi = 0$. In addition, the triangular sediment wedge geometry implies

$$C = \frac{h_b^2}{2\tan\beta}, \quad \frac{\partial h_b}{\partial s} = \frac{\tan\beta}{h_b}\frac{\partial C}{\partial s}, \quad h_b = B\tan\beta. \tag{2.12}$$

This assumes that β is constant. Alternatively, we might suppose B is constant; in that case,

$$C = \tfrac{1}{2}Bh_b, \quad \frac{\partial h_b}{\partial s} = \frac{2}{B}\frac{\partial C}{\partial s}, \quad h_b = B\tan\beta. \tag{2.13}$$

In the first case, equation (2.11) can be written in the form

$$q = K\left[0.28\rho_w g h_w \sqrt{C\tan\beta}\frac{\partial h}{\partial s} - \Delta\rho\, g D_s \frac{\partial C}{\partial s}\right]; \tag{2.14}$$

in the second, it takes the form

$$q = K\left[\frac{0.4\rho_w g h_w C}{B}\frac{\partial h}{\partial s} - 2\Delta\rho\, g D_s \frac{\partial C}{\partial s}\right], \tag{2.15}$$

and we use this as it is somewhat algebraically simpler.

Ashton & Murray [46] compare various recipes for along-shore transport, most of which replace the $\sin(\phi+\theta)$ dependence in equation (2.11) with a proportionality to $\sin(\phi+\theta)\cos(\phi+\theta)$, apparently due to this factor appearing in the along-shore momentum flux [42, eqn. (13)], and its use by Bowen [47] in constructing a model for the along-shore current, although Longuet-Higgins (eqn. (53)) finds no such dependence. By writing the shore-line evolution equation as an Exner-type equation, Ashton and Murray suggest that the gradient of the along-shore flux provides a diffusion term for the shore-line evolution, but this seems problematical.[3]

It should be pointed out that while the along-shore transport term seems sensible for $-\pi/2 < \theta < \pi/2$, its extension to embayments in which θ goes beyond this range is open to question,

[3]Because the shore-line evolution equation is given by an interfacial velocity due to erosion, not by a conservation law: it is the offshore sediment which is conserved.

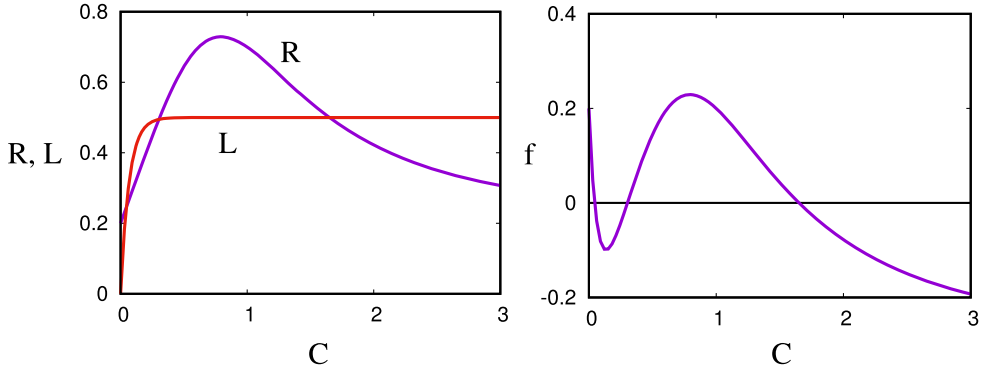

Figure 4. Qualitative form of the Limber–Murray functions L and R and the difference function $f(C) = R(C) - L(C)$. The choice of functions used here is entirely schematic and the units are arbitrary. As explained in the text, we have replaced Limber and Murray's discontinuity in L with a sharply rising function, and we have subsumed the shoreward transport rate λC_0 into $R(C)$. Neither of these affects the discussion.

but we retain the expression as is for the moment. Putting it all together, we obtain from equations (2.8) and (2.15),

$$C_t = R(C) - \lambda(C - C_0) + DC_{ss} - K_0(Ch_s)_s, \tag{2.16}$$

where

$$R(C) = rCA(C), \quad K_0 = \frac{0.4\rho_w g h_w K}{B}, \quad D = 2K\Delta\rho\, g D_s, \tag{2.17}$$

and this is coupled with the cliff evolution equation in equation (2.2), which takes the form

$$v_n = \frac{R(C)}{H}; \tag{2.18}$$

the erosion function $R(C)$ increases at first with C, and then decreases; an example is shown in figure 4. The shape of this function can be compared favourably with fig. 7 of Sunamura [48], although the experimental data used there are for soft rock cliffs. The rest of this paper deals with this model. As we shall see, it is the rubble-enhanced erosion rate (R increasing) which enables instability, whereas the armouring effect (R decreasing) promotes stability.

3. The Limber–Murray model

As promised, we now return to a discussion of the model of Limber & Murray [40], though its form is given more explicitly by Limber & Murray [29]. The model we present here is similar to the Limber–Murray model, with the exceptions that our diffusion is with respect to along-shore distance s, there is a difference in the seaward loss term, and we include a curvature-dependence of the erosion rate. Note that there is a missing minus sign on the left-hand side of Limber & Murray's [40] eqn. (1). The Limber–Murray beach width w is replaced by our sediment concentration C, but essentially the two variables are treated similarly, with an approximate identification $C = h_b w$. Our appeal to along-shore sediment flux relies on the mechanism for this provided by Komar [38], although that relies on the Longuet-Higgins theory for fairly calm flows on a beach. However, it seems reasonable to use this term at least until caves or inlets start to form.

Limber & Murray [40] took R to be a function shaped as in figure 4.[4] Non-zero weathering at $C = 0$ implies $R(0) > 0$, and then R increases for small C, but reaches a maximum and decreases

[4]With some inconsequential modifications. They took $R(0) > 0$ and $R(\infty) = 0$, and also $L(0) = 0$, $L(C) = S =$ constant for $C > 0$. In drawing figure 4, we have used equation (2.16) to subsume the shoreward transport term λC_0 into R, so that $R(\infty) > 0$, and we have replaced Limber and Murray's discontinuous L with a steeply rising function. Neither of these adjustments makes any difference to the discussion.

for large C. In the case of beach width, the decrease is due to cliff shielding by a large beach. In the present case, similar armouring should occur. Increasing C leading to a talus slope will shield the cliff and effectively reduce R towards zero.

In the Limber–Murray model, the loss term which we have taken as a linear expression $L(C) = \lambda(C - C_0)$ is taken as a constant, $L(C) = S$ (more precisely $h_b S$), without any particular motivation. This cannot be entirely accurate, since if $C = 0$, we must have $L(0) = 0$. In their 2011 simulations, they necessarily assume this, so that in fact their choice of L is discontinuous; a better choice might be a steeply increasing function. In figure 4, we illustrate qualitative choices of R and L similar to those chosen by Limber and Murray, and we also show the consequent function $f(C) = R(C) - L(C)$.

The Limber–Murray sediment flux is motivated by the same Longuet-Higgins-inspired derivation, but is presented rather differently. Their 2011 eqn. (3) is actually equivalent to our equation (2.16) under the identification $C = h_b w$ and $D = K_0 w$. In their 2011 simulation, figure 3, the solution evolves to patches with beaches and patches with no beach; and yet there is still an offshore sediment flux (the term $L(C)$), even when there is no beach! The resolution of this lies in the necessary fact that when the beach disappears, there must be a submerged beach [41, fig. 3], and this implies that the basic sediment variable is more like our C (but no longer taken as $h_b w$), in which case the details of the functions R and L would change. Having said all that, the principal difference between Limber–Murray and our model lies in the diffusion along arc length, and in the choice of the loss function L. We analyze the consequences of this in the following section.

(a) Analysis of the Limber–Murray model

After a long time in their model simulations ([29], figure 3), the Limber–Murray coastline has broken up into a series of horizontal cliffs with beaches, and a series of roughly semi-circular headlands without beaches.

For the horizontal cliffs, we may take $h_s = 0$, and then the resulting model for C is simply

$$C_t = f(C) + DC_{ss}, \tag{3.1}$$

and is of Fisher or more precisely FitzHugh–Nagumo type [49], and its behaviour is well understood. Taking the form of $f(C)$ to be as shown in figure 4, there are three equilibria $C_1 < C_2 < C_3$, which are the roots of $f(C) = 0$, of which the lowest (C_1) and highest (C_3) values are stable. To compare with Limber & Murray's [29] figure 3, illustrating pocket beaches and rocky headlands, we interpret $C = C_3$ as a beach and $C = C_1$ as a rocky shore. For a spatially varying initial state, high values tend to the upper stable state, while low values tend to the lower stable state ($C_1 \approx 0$), thus forming a sequence of platforms where $C \approx C_1$ and $C \approx C_3$. These platforms are joined by wave fronts which move at a speed v. The waves are described by putting $\zeta = s - vt$ and seeking solutions $C(\zeta)$, whence C satisfies

$$-vC' = f(C) + DC'', \tag{3.2}$$

where the prime denotes differentiation with respect to ζ. Suppose for example that a beach lies to the right of a rocky headland. Then the appropriate boundary conditions for equation (3.2) are $C \to C_1$ as $\zeta \to -\infty$, and $C \to C_3$ as $\zeta \to \infty$. The value of v is determined as the unique value which joins the saddle $(C_1, 0)$ in the (C, C') phase plane to the saddle $(C_3, 0)$. Multiplying by C' and integrating across a wave front, we find

$$v = -\frac{\int_{C_1}^{C_3} f(C)\,\mathrm{d}C}{\int_{-\infty}^{\infty} C'^2\,\mathrm{d}\zeta}, \tag{3.3}$$

and thus the sign of the wave speed is opposite to that of $\int_{C_1}^{C_3} f(C)\,\mathrm{d}C$. Suppose, for example, as suggested in figure 4, that this integral is positive; for a given erosion function $R(C)$, this is the case if $L(\infty) = S$ is sufficiently small. Then a wave joining headland to beach will move towards the headland, and eventually the entire shore-line will become beach. If S is sufficiently large, so that

the integral is negative, then the entire shore will eventually become rocky. In more generality, this kind of transient approach to the final state will only occur if $R(0) \lesssim S \lesssim \max R$, so that there are indeed three equilibria.

The purpose of our analysis of the Limber–Murray model is to explain how their numerical results can be understood in terms of their model formulation. In particular, their prescription of the loss function $L(C)$ allows the (temporary) formation of alternating pocket beach/rocky headland shore-lines. This is due to the assumption that $L(C)$ saturates at large C. We do not make this assumption; not because it is necessarily inappropriate, but because our focus is on the nonlinear evolution of the shore-line profile itself.

4. Instability

In their 2011 simulations, Limber and Murray started with an irregular coastline and no beaches. The oscillating curvature (hauling f up and down in equation (3.1)) allowed beaches to form patchily, and some headlands were able to endure. A more natural initial condition might be to start with a flat coast and a non-uniform beach cover (if you are trying to form headlands, best not to start with them already there). But in this case, with $h_{ss} = 0$ everywhere, C will jump to form patchy beaches as before, and as before, we have the beach recession rate $v_b = R(C_3)/H$ greater than the rocky shore recession rate $v_h = R(C_1)/H$ (see equation (2.18)), and headlands should start to form. There is then a competition between how fast the headlands can grow and how long it takes for the uniform beach/bare state to prevail; this depends on the various parameters in the problem, but the issue is not pursued here.

In any event, the underlying theme is that we would like the steady, uniform growth state to be unstable, and we now examine this for the present model. To begin with, we make the model dimensionless. Before doing so, we make one further adjustment. It is a common feature in interfacial growth models that the hyperbolic interfacial growth equation[5] allows shocks to form, corresponding to jumps in interfacial slope. This is well known in crystallization (e.g. [55, p. 320]). In crystallization, the shocks are alleviated by a surface energy term, whose effect in equation (2.18) would be to add a 'cliff exposure' term proportional to the curvature κ to the right-hand side. The curvature is defined as

$$\kappa = \frac{h_{xx}}{(1 + h_x^2)^{3/2}} = \frac{h_{ss}}{x_s}. \tag{4.1}$$

With this in mind, we modify the growth rate to be

$$R(C) \to R(C)(1 + l_c\kappa). \tag{4.2}$$

What could provide such an effect in the present case? The simplest answer to this, if we consider the effect of the geometry in figure 2, is that the shelter of the inlet will reduce the efficacy of the erosive wave action of the sea, and exposure of a protruding headland will increase it. The simplest, though crude, representation of this is to suppose that the erosion coefficient r in equation (2.6) is a monotonically increasing function of κ, and this would lead to a modification of the function R as in equation (4.2).

For our model, we take $f(C) = R(C) - \lambda C$ in equation (3.1) (the term λC_0 can be absorbed into R). We take the model from equations (2.16) and (2.18), but using the cliff exposure term in equation (4.2); in fact the argument about ocean efficacy for erosion has the same implication for removal rate $L(C)$, so we modify this term similarly; thus the model is

$$\begin{aligned} C_t &= [R(C) - \lambda C](1 + l_c\kappa) + DC_{ss} - K_0(Ch_s)_s, \\ v_n &= E = \frac{R(C)(1 + l_c\kappa)}{H}. \end{aligned} \tag{4.3}$$

[5]In various contexts, this is known as the eikonal equation (e.g. [50]); it occurs in different forms as the Hamilton–Jacobi equation [51, p. 155], in reaction–diffusion theory [52, 53, p. 166], and in ray theory (e.g. [54]). The simplest pedagogical example is that of determining the shape of a sandpile (with constant slope angle), a problem which can be solved explicitly using Charpit's method.

(a) Non-dimensionalization

Non-dimensionalization of the model is not so easy as the parameters are not well constrained. We start by supposing that cliff height $H \sim 50\,\mathrm{m}$ [4; 6, p. 274], and that the debris depth $h_b \sim 3\,\mathrm{m}$. This quantity does not seem easy to determine. For one thing, we can expect the debris pile to accumulate during cliff collapse following storms, and dissipate thereafter. Modelling it as a time-averaged (or storm-averaged) quantity as we do belies this reality. In this, modellers face the same problem as in the description of river flow, where the flood hydrograph consists of a series of storm-induced spikes followed by relaxation towards low stage. A more pungent example is that of landscape erosion [56], where one models rainfall as constant, and (worse) erosion as a function only of mean water depth.

One approach is to take the example of the Twelve Apostles [4], where the stacks lie on the order of 100 m from the cliff and in up to 10 m water depth. Since at least some of the inlets along this coast have exposed beaches, we might estimate $h_b \sim 10\,\mathrm{m}$ and $\tan\beta \sim 0.1$ (see equation (2.12)), whence we would have a typical wedge cross-sectional area $C_v \sim h_b^2/2\tan\beta$ (see equation (2.12)) $\sim 500\,\mathrm{m}^2$. The trouble with this is that the beaches are sandy, so that our model can not really apply unless we include comminution, and further, the transport properties of sand are likely to be very different to those of coarse boulders.

A better example may be that of the boulder beach studied by Gómez-Pazo *et al.* [57]. This appears to be a 'fossil' beach, resting on a shore platform, in which cliff erosion has ceased, and the beach is in a stationary state. Storms cause motion of the boulders, but there appears to be no net flux. The slope ranges from 7 to 12°, so we might take $\tan\beta \sim 0.15$, and the beach extent B is 20 m, which would imply $h_b \sim 3\,\mathrm{m}$. We assume these values, and consequently a typical value of C is $C_v \sim 30\,\mathrm{m}^2$.

Next, we assume a typical retreat rate $v_n \sim 0.1\,\mathrm{m\,yr^{-1}}$. This seems quite a high erosion rate, but is based on the notion that Bishop's Island in figure 1 has ruins of an early Christian monastic site, thus dating its connection to the mainland at $\lesssim 1500\,\mathrm{yr}$, and it is presently 100 m offshore. In fact, this is a typical rocky cliff retreat rate. Shadrick *et al.* [58] give values of approximately $0.06\,\mathrm{m\,yr^{-1}}$, Regard *et al.* [59] give an average European value of $0.03\,\mathrm{m\,yr^{-1}}$, Gómez-Pazo *et al.* [60] give $0.11\,\mathrm{m\,yr^{-1}}$ for a cliff in Galicia, while the retreat rate for the Twelve Apostles is $0.22\,\mathrm{m\,yr^{-1}}$ [4].

With the above estimates, we suppose from equation (4.3) that $R \sim Hv_n \sim 5\,\mathrm{m^2\,yr^{-1}}$. As above, $C \sim C_v \approx 30\,\mathrm{m}^2$. Since in the steady state, $R \sim R_0 \sim \lambda C$, this suggests $\lambda \sim 0.2\,\mathrm{yr^{-1}}$. We find that it is the term in K_0 in equation (4.3) which drives the instability, so we choose a length scale l for both h and s by balancing this term with the erosional source term, thus

$$l = \frac{K_0 C_v}{R_0}. \tag{4.4}$$

We choose a time scale determined by cliff erosion rate. Our choice of scales for the variables is then

$$\begin{aligned} &R \sim R_0 \sim 5\,\mathrm{m^2\,yr^{-1}}, \quad C \sim C_v \sim 30\,\mathrm{m}^2, \quad h, s \sim l, \\ &t \sim t_0 \equiv \frac{lH}{R_0}, \quad v_n \sim \frac{R_0}{H}, \quad \kappa \sim \frac{1}{l}, \end{aligned} \tag{4.5}$$

and the corresponding dimensionless equations (retaining the same notation for the variables) are

$$\begin{aligned} \delta C_t &= [R(C) - \Lambda C](1 + \varepsilon\kappa) + \nu C_{ss} - (Ch_s)_s, \\ v_n &= \frac{h_t}{(1 + h_x^2)^{1/2}} = R(C)(1 + \varepsilon\kappa), \end{aligned} \tag{4.6}$$

where the dimensionless parameters are given by

$$\varepsilon = \frac{l_c}{l}, \quad \Lambda = \frac{\lambda C_v}{R_0}, \quad \nu = \frac{DR_0}{K_0^2 C_v}, \quad \delta = \frac{R_0}{K_0 H}. \tag{4.7}$$

The dimensionless form of κ is still given by equation (4.1).

It remains to choose the cliff exposure length l_c, the sediment transport parameter K_0 and the diffusivity D. We shall have more to say about the curvature dependence of erosion in §6, but in its present form, it implies that erosion will cease at a semi-circular indentation of radius l_c, which we might associate with the size of the eroded boulders. It is a very imprecise quantity, and we choose $l_c \sim D_s = 1$ m; it clearly needs to be smaller than commonly observed inlets such as that in figure 2, and its precise value is not important if it is sufficiently small.

The transport parameters K_0 and D are less accessible. We circumvent this by choosing a value $K_0 \sim 42\,\mathrm{m\,yr^{-1}}$, in order that the resulting length scale $l \sim 250$ m, which corresponds to the observed coastline corrugation length scale which appears relevant on the Loop Head peninsula, and is also the embayment length scale at the Twelve Apostles (obtained from Google Earth, 13 embayments over a distance of 3.3 km from the Razorback to the Twelve Apostles viewpoint, approximately); cf. Bezore *et al.* [4, fig. 8]), and also Felton [61, figs. 1 and 2].

With this value of K_0, we can use equation (2.17) to compute $K = 0.02\,\mathrm{m^2\,Pa^{-1}\,yr^{-1}}$ and $D \sim 840\,\mathrm{m^2\,yr^{-1}}$. We might for interest compare the value of K with an equivalent value from the Meyer-Peter/Müller relation, but it is found that the latter is six orders of magnitude higher. This is perhaps not so surprising, given the particle displacement rates on the boulder beach of Gómez-Pazo *et al.* [60] of $\sim 3\,\mathrm{m\,yr^{-1}}$, as compared to sandy beach transport rates which are much higher.

It is natural to ask what would happen to our theory if we allowed different grain sizes to occur via comminution. The simplest suggestion would be that it is the largest boulders which are rate-controlling in the erosion process. But the process of comminution will cause eventual evolution to sand, so there is a question of competition between the erosional and comminution time scales. As for the theory, we expect K to increase as D_s decreases, and the effect on the parameters is to reduce both ε and ν, and this does not compromise our discussion of stability below.

Limber & Murray [29] relate K_0 and D by the recipe:

$$K_0 = \frac{D}{B}, \tag{4.8}$$

(interpreted from their eqn. (3)), which gives the same result as our prescription here. However, their diffusion coefficient is $D \sim 10^7\,\mathrm{m^2\,yr^{-1}}$, but like the other papers cited, their concern is with the transport of beach sand. A Meyer-Peter/Müller type of value for K can explain this high value, but in fact Limber and Murray appear not to provide a basis for their choice.

It is worth dwelling on this a little further. Eqn. (3) of Limber & Murray [29] takes the form

$$w_t = \frac{2H}{h_b}\frac{\partial \eta_c}{\partial t} + D_0 \frac{\partial^2 \eta_b}{\partial s^2} + S, \tag{4.9}$$

in which we have interpreted the coefficient of $\partial\eta_c/\partial t$ in terms of their description and our notation; we have also written the diffusive second derivative term with respect to arc length s rather than x. In this equation, w is the (variable) beach width, η_b is the location of the beach edge (where it meets the shore platform) and η_c is the location of the cliff, on an η axis which is orthogonal to the x axis. They do not say in which direction it points, but it is apparent that it must point seawards, so that $\eta_b = \eta_c + w$.

There is some ambiguity of signs, but we must have $\partial\eta_c/\partial t = -E$, where E is the erosion rate (despite their eqn. (1)). Then if we multiply equation (4.9) by $\frac{1}{2}h_b$ (taken here as constant), we derive in our notation

$$C_t = R - L + D_0 C_{ss} - \frac{D_0 C}{B} h_{ss}, \tag{4.10}$$

which is essentially our equation (2.16), and we have identified $\frac{1}{2}h_b S = -L$.

Although the Limber–Murray model is thus essentially the same as ours, the flux term $-D_0\partial\eta_b/\partial s$ is formulated quite differently, supposing the flux is proportional to the gradient of beach edge. Limber and Murray refer back to their earlier paper [46], but that had a flux proportional to shore-line gradient; but neither appears to have any physical basis, and no

Table 1. Assumed values of dimensional and consequent dimensionless parameters. The choice of h_b and B corresponds to $\tan\beta = 0.15$, or $\beta = 8.5^\circ$.

parameter	typical value	parameter	typical value
B	20 m	K_0	42 m yr^{-1}
C_v	30 m^2	l	250 m
D	840 m^2 yr^{-1}	l_c	1 m
D_s	1 m	R_0	5 m^2 yr^{-1}
g	9.8 m s^{-2}	t_0	2500 yr
h_b	3 m	$\Delta\rho$	2×10^3 kg m^{-3}
h_w	10 m	λ	0.2 yr^{-1}
H	50 m	ρ_w	10^3 kg m^{-3}
δ	0.002	Λ	~ 1
ε	0.004	ν	0.08

justification for the choice of D_0 is given. It is remarkable that we have arrived at a structurally similar model by a completely different route.

In summary, our choice of parameter values is listed in table 1, which also includes the consequent values of the dimensionless parameters.

(b) Intrinsic coordinates

It is convenient (indeed, essential) to use intrinsic coordinates s, t rather than x, t. Thus we consider $x = x(s,t)$ and $h = h(s,t)$ and define $\mathbf{r}(s,t) = (x,h)$. Various expressions follow on changing coordinates, and also using the Serret–Frenet formulae. With $\mathbf{t}$ and $\mathbf{n}$ being unit tangent and normal vectors, we have

$$h_s = h_x x_s, \quad \mathbf{t} = (x_s, h_s), \quad \mathbf{n} = (-h_s, x_s), \quad \kappa = \frac{h_{ss}}{x_s} = -\frac{x_{ss}}{h_s}, \tag{4.11}$$

and the normal velocity condition in equation (4.6)$_2$ becomes

$$\mathbf{r}_t.\mathbf{n} = E = R(C)(1 + \varepsilon\kappa). \tag{4.12}$$

Note that the issue flagged previously for equation (2.2) concerning the direction of retreat disappears in Serret–Frenet terms, since the normal $\mathbf{n}$ always points to the left of the $\mathbf{r}$ curve as s increases. In general, we can thus write

$$\mathbf{r}_t = E\mathbf{n} + U\mathbf{t}; \tag{4.13}$$

if we differentiate this with respect to s, dot with $\mathbf{t}$, and use the fact that $\mathbf{t}$ is a unit vector (and orthogonal to $\mathbf{n}$), we find that U satisfies

$$U_s = \kappa E. \tag{4.14}$$

Together with equations (4.6), equations (4.13) and equations (4.14) provide a closed system for $\mathbf{r}$ and C.

It is convenient to write equation (4.13) in terms of the complex variable $z = x + ih$, not the least because the expressions in equation (4.11) show that

$$\kappa = -\frac{iz_{ss}}{z_s}, \tag{4.15}$$

which is better than the expressions in equation (4.11) as it avoids potential singularities. Equation (4.13) then takes the form

$$z_t = (U + iR)z_s + \varepsilon R z_{ss}, \tag{4.16}$$

with U determined by quadrature of

$$U_s = -\frac{iEz_{ss}}{z_s}. \tag{4.17}$$

Further reduction is possible. Since κ is real and since $|z_s| = 1$ by definition of arc length, it follows that

$$z_s = \mathrm{e}^{\mathrm{i}\theta}, \tag{4.18}$$

and θ is just the slope angle of the coastline. Hence, also from equation (4.15),

$$\kappa = \theta_s. \tag{4.19}$$

Using these in equation (4.17) and then taking the s-derivative of equation (4.16) yields the alternative pair of equations for U and θ,

$$\begin{aligned} \theta_t &= R_s + U\theta_s + \varepsilon(R\theta_s)_s, \\ U_s &= R\theta_s(1 + \varepsilon\theta_s). \end{aligned} \tag{4.20}$$

The model reduces to solving these for θ and U, together with the equation for C in equation (4.6), which now takes the form

$$\delta C_t = [R(C) - \Lambda C](1 + \varepsilon\theta_s) + \nu C_{ss} - (C\sin\theta)_s. \tag{4.21}$$

The shape of the coastline can then be recovered by integrating equation (4.18).

(i) Boundary and initial conditions

The model equations have a solution corresponding to the retreat of a planar cliff. This solution has $U = \theta = 0$, $C = C^*$, where C^* is the unique solution of $R(C^*) = \Lambda C^*$. The retreat rate is determined by equation (4.16), and is $h = R(C^*)t$, and more generally, $z = s + iR(C^*)t$. On an infinite domain, it is then natural to apply boundary conditions corresponding to this steady state at the ends; thus we prescribe

$$\theta \to 0, \quad C \to C^* \quad \text{as} \quad s \to \pm\infty, \quad U \to 0 \quad \text{as} \quad s \to -\infty; \tag{4.22}$$

the condition on U is arbitrary. The initial conditions for C and θ should also satisfy these boundary conditions, and then normally will be subjected to a localised perturbation in θ or C or both. In our numerical solutions in §5, we take advantage of the symmetry of the model (θ and U are odd in s, while C is even) to solve the model on a half-range, thus with

$$\theta = C_s = U = 0 \quad \text{on} \quad s = 0. \tag{4.23}$$

(c) Stability calculation

We now study the stability of the basic state $\theta = 0$, $C = C^*$. We put $C = C^* + \phi$, so that the linearized model takes the form

$$\begin{aligned} \theta_t &= R'\phi_s + \varepsilon R\theta_{ss}, \\ \delta\phi_t &= (R' - \Lambda)\phi + \nu\phi_{ss} - C\theta_s, \end{aligned} \tag{4.24}$$

where R, R' and C are all evaluated at $C = C^*$.

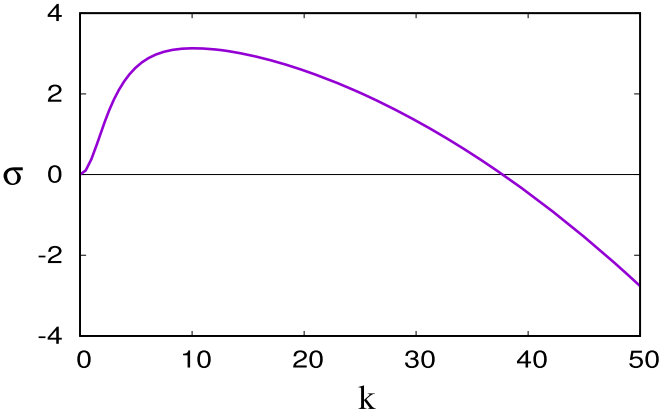

Figure 5. Plot of the unstable root of equation (4.25) using values $\Lambda = 1.29$, $R' = 0.59$, $\delta = 0.002$, $\nu = 0.08$, $\varepsilon = 0.004$, $R = 0.644$ (R, R' and C correspond to values used in the numerical solution below).

We assume that $\Lambda > R'$ at the steady state. Solutions are proportional to $e^{iks+\sigma t}$, and this leads to

$$\sigma = -\varepsilon R k^2 + \frac{R' C k^2}{\Lambda - R' + \nu k^2 + \delta\sigma}; \tag{4.25}$$

the stable root is $\sigma_- \approx -(\Lambda - R' + \nu k^2)/\delta$, while the unstable (slow) root, assuming $\delta \ll \nu$, is uniformly approximated by

$$\sigma_+ = -\varepsilon R k^2 + \frac{R' C k^2}{\Lambda - R' + \nu k^2}. \tag{4.26}$$

The growth rate rises to a maximum $\sigma_+ \sim R'C/\nu$ for $k \sim 1/\nu^{1/2}\varepsilon^{1/4}$, and then slowly subsides for larger k. Figure 5 shows an example.

What of the Limber–Murray model, as in figure 4? Here the right-hand steady state (permanent beach) is in fact stable. However, the left-hand steady state (bare cliff) is unstable. If we try and approach the discontinuous L that Limber and Murray adopt, this corresponds to letting $\Lambda \to \infty$ in equation (4.26); in this limit the growth rate approaches zero. Although hazardous to make statements about discontinuous systems, we think that the discontinuous model is more accurately represented by the sharply rising L in figure 4, and thus in practice the instability is suppressed by its very slow growth rate.

5. Numerical results

It is straightforward to step the diffusive equations for C and θ forward in time. We used a fully implicit finite difference method with time step $\Delta t = 0.001$ and space step $\Delta s = 0.01$. Because of the reflectional symmetry under $\theta \to -\theta$, $s \to -s$, $x \to -x$, $C \to C$, $U \to -U$, we solved the problem on the half range $0 < s < s_{\max}$, with $\theta = C_s = U = 0$ on $s = 0$, and $\theta = 0$, $C = C^*$ on $s = s_{\max}$. The code was written in Fortran 77, and the output files fed into a MATLAB script to produce the graphical output. The code ran in approximately 25 s. The Fortran code and the MATLAB script are provided as electronic supplementary material. For those unable to run Fortran, we also provide the data files used to produce the figures (as the last frames of movies).

The initial condition was a localized (near $s = 0$) perturbation for θ, whose effect then spread out, creating a sequence of headlands and inlets as shown in figures 6 and 7. The model is therefore successful in producing an irregular coastline, but it has not as yet provided evidence of its ability to produce self-intersecting shore-lines, which would then be interpreted as cave formation, consequently leading to cliff collapse and hence sea stacks.

There are two questions one might ask about the solution in figures 6 and 7. The first, naturally, is to enquire what happens at different parameter values. There are four dimensionless

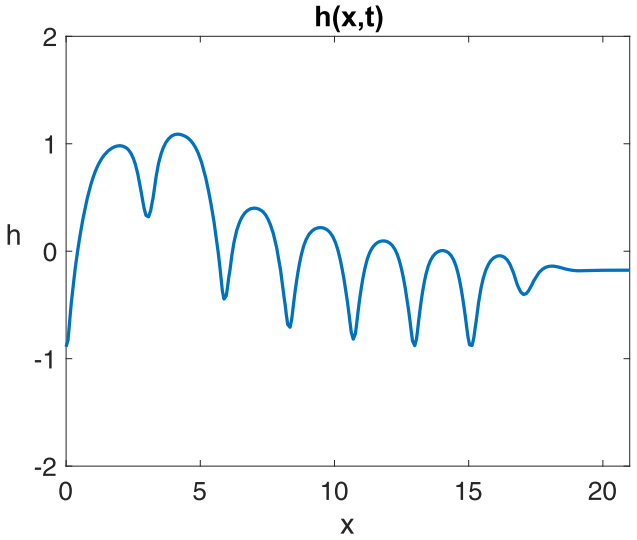

Figure 6. h as a function of x, obtained by solving equations (4.20) and (4.21) on $0 < s < 30$, using values $\delta = \varepsilon = \nu = 0.1$, $C^* = 0.5$ corresponding to $\Lambda = 1.29$ (a value of $C^* < 0.79$ is necessary so that $R'(C^*) > \Lambda$ for the function $R(C) = 0.2 + C/(1 + C^3)$ which is used here). The solution was obtained up to $t = 20$, and normalized so that the mean of h (in s) is zero, and this is the corresponding profile at $t = 20$. Note that the x scale is foreshortened from the original s interval length.

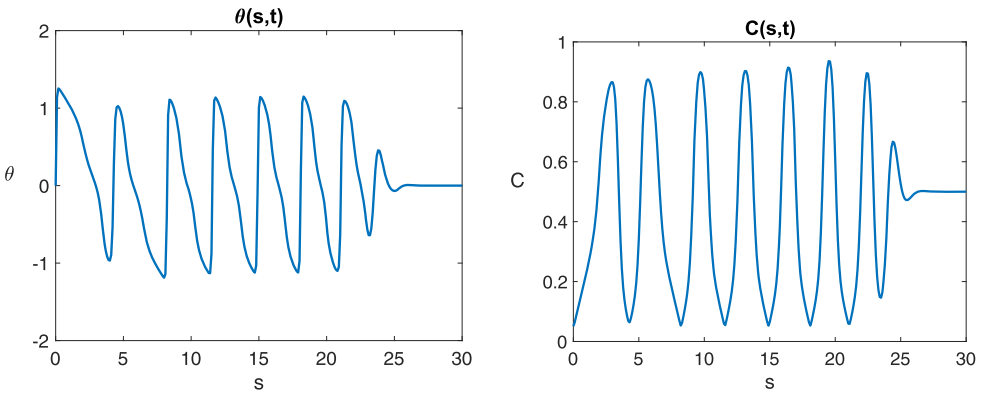

Figure 7. Solutions for θ and C as functions of s (not x), corresponding to the solution in figure 6.

parameters in the model: δ, ε, Λ and ν. In addition, the shape of the erosion function can be largely captured by the position of its maximum, say $R = R_M$ at $C = C_M$.

Now the parameters ε, δ and ν are all small, and are singular perturbation coefficients, and they control boundary-layer behaviour. Of these, ε and δ are reliably small, and with our definitions in equations (2.17) and (4.4), we can write

$$\nu = \left(\frac{D_s}{0.2 h_w} \frac{\Delta\rho}{\rho_w} \right) \frac{B}{l}, \tag{5.1}$$

and the term in brackets approximate 1; so we regard it as safe to take ν to be small also.

It is possible to analyze the solutions on the assumptions that ε, δ and ν are all small, and the consequences of this analysis are illustrated in figure 7. The solution tends to a steady state in which θ and C oscillate, and θ has periodic shocks, smoothed as is evident in equation (4.20) when $\varepsilon > 0$. At the shocks in θ (headlands) where θ jumps up, there are singular layers in C, where the

slope C_s changes rapidly. So the only parameters which might affect the behaviour are R_M, C_M and Λ.

But in fact the boundary-layer analysis indicates this is not so, and the structure of the solution in figures 6 and 7 remains valid, although of course quantitative aspects (amplitude, period) will vary; in other words, the behaviour of the solution in figures 6 and 7 is typical for the whole range of plausible parameter values. We have confirmed this by solving the model with an erosion rate given by

$$R = R_0 + \frac{3(R_M - R_0)u}{2 + u^3}, \quad C = C_M u, \tag{5.2}$$

which has a maximum of R_M at $C = C_M$, and $R(0) = R(\infty) = R_0$. The choice used in figure 6 (and also portrayed in figure 4) corresponds to this form, with $C_M \approx 0.79$ and $R_M \approx 0.73$. Instability then occurs for $\Lambda > R_M/C_M$, and for such values the solutions are qualitatively similar to figures 6 and 7 as we vary C_M and R_M.

The second question is whether there are any coastlines that actually look like figure 6. On the face of it, we should not expect such regularity. For a start, the model is very idealistic, ignoring practical issues such as topographic variation of the land domain, stratigraphic and lithological variability, storm variability in both direction and strength, as well as the local fluctuations associated with turbulent storm impact. The best we might hope for is a lumpy shore-line profile, and the Loop Head peninsula provides a good example of this.

But in fact there are coastlines which have a degree of regularity, and which do resemble the regular pattern of figure 6. The coastline near the Twelve Apostles has such regularity, with pointed headlands [4, fig. 8], although the comparison is a bit devious, since in our terms, the modelled coastline should have developed self-intersections (and hence stacks), so that the pointed headlands are remnants of this process.

A better example may be that of a coastline on one of the Hawaiian islands, Lanai [61, figs. 1 and 2], which is lumpy but regular. Despite such similarity, it would be a hazardous suggestion to say that the present theory can explain such coastlines, at least in a quantitative way.

6. Discussion and conclusions

We have provided a model which can explain the spatial instability of eroding cliff shore-lines. The model is similar in concept to that of Limber & Murray [40], which we have discussed extensively, but it differs in several important aspects. The first is that our formulation of erosion and sediment removal, although superficially similar, leads to different dynamics. A more fundamental distinction is that our along-shore transport terms lead to spatial derivatives in terms of arc length. In principle, this allows the possibility of self-intersecting shore-lines, and our interpretation of a headland which bends back to intersect itself would be cave formation and thus (after collapse of the cliff arch) formation of a sea stack.

All that is necessary in our model to facilitate this bend-back is that the oscillations in θ which are shown in figure 7 should have extremes which go beyond $\pm\pi/2$. Of course, that does not guarantee self-intersection, but it allows the possibility. There are two ways of trying to adjust the model to enable this.

One is the assumed form of the 'cliff exposure' term $l_c\kappa$ in equation (4.2). Let us define the cliff erosional factor to be E_c, which in the case of equation (4.2) or, when written dimensionlessly as in equation (4.6), is

$$E_c = 1 + \varepsilon\kappa. \tag{6.1}$$

The first thing to say is that we posited this term because the mathematical model seems to require such a term in order to smooth the shocks (jumps in shore-line slope) which occur, and experience in other physical situations (gas dynamics, water waves, crystal growth) suggests that such regularizing terms commonly exist. More generally, we just require $\partial E_c/\partial\kappa > 0$. Now, a boundary-layer analysis of equations (4.20) and (4.21) shows that in the shocks where θ jumps,

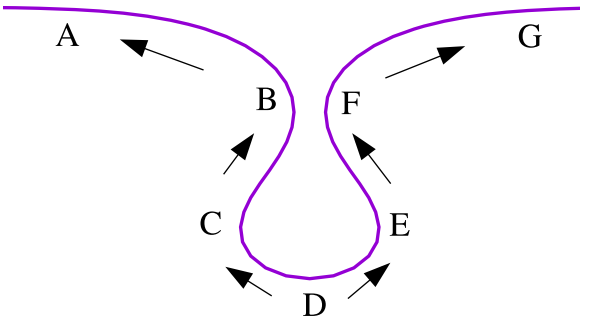

Figure 8. The coastline profile $h(x)$ computed on the assumption that $\theta = A\exp(-bs^2)\sin s$, $A = 3.8$, $b = 0.5$. The arrows indicate the direction of the shore-line flux, according to equation (6.3).

$\varepsilon\kappa \sim 1$, which allows the unphysical possibility that $E_c < 0$. Such a possibility is easily eliminated by choosing, for example, $E_c = e^{\varepsilon\kappa}$.

A more serious objection to equation (6.1) is that it does not take account of embayment. In a bay where $\kappa < 0$ over an extended length of shore-line ($\sim 1/\kappa$), the shore is sheltered, and this suggests the possibility that E_c is determined non-locally due to embayment hydrodynamics, for example as a function of a convolution integral,

$$E_c = E_c\left[\int_{-\infty}^{\infty} G(\xi)\kappa(s-\xi)\,\mathrm{d}\xi\right], \tag{6.2}$$

where the kernel G would be an even function, in order to preserve the invariance of the model under the transformation $s \to -s$, $\theta \to -\theta$.

The other issue is with the along-shore sediment flux:

$$J = C\sin\theta. \tag{6.3}$$

In a forming stack such as shown in figure 8, equation (6.3) suggests the flux is directed as indicated by the arrows. There are two issues here. The first is that in the model we have assumed a wave motion orthogonal to the coast. Strictly then, BC and EF are sheltered and there would be no sediment flux. In reality, storms come in at a variety of angles, there are turbulent fluctuations, so that the model might be better described by taking, for example,

$$J = C\int_{-\pi/2}^{\pi/2} k(\phi)\sin(\theta+\phi)\,\mathrm{d}\phi, \tag{6.4}$$

where the distribution $k(\phi)$ describes the directional variety of incoming storm waves. In addition, we might drop the flux to zero if $|\theta + \phi| > \pi/2$. In particular the directions in AB and FG should be reversed, which then allows the positive feedback to occur in these indentations. Also, attention needs to be paid to the case of a forming oxbow (reverse the sign of A in figure 8), since in that case the flux should be inconsequential. Thus J should depend also on coastline shape, which is perhaps most simply represented by curvature, possibly in a convolution form as in equation (6.2).

In summary, we think the formulation of the present model provides a suitable platform from which to pursue our goal of providing a dynamic mechanism for sea stack formation, but there are many aspects of the modelling which require further scrutiny, and we hope to develop these in a future publication.

Data accessibility. The file esm.zip contains the codes used in generating the numerical solutions.

The data are provided in electronic supplementary material [62].

Declaration of AI use. We have not used AI-assisted technologies in creating this article.

Authors' contributions. A.F.: conceptualization, methodology, software, writing—original draft, writing—review and editing; F.N.: software, writing—review and editing; G.K.: software.

All authors gave final approval for publication and agreed to be held accountable for the work performed therein.

Conflict of interest declaration. We declare we have no competing interests.

Funding. G.C.K. and F.S.L.N. acknowledge the financial support of A.C.F., who in turn acknowledges the logistical support of G.C.K. and F.S.L.N. in organising the International Symposium on The Edges of Glaciology, Limerick, 2–7 July 2023, where the inspiration for this paper occurred. A.C.F. also acknowledges the support of the Mathematics Applications Consortium for Science and Industry (www.macsi.ul.ie) funded by the Science Foundation Ireland mathematics grant no. 12/IA/1683.

References

1. Duff PMLD. 1993 *Holmes' principles of physical geology*, 4th edn. London: Chapman & Hall.
2. Trenhaile AS. 1987 *The geomorphology of rock coasts*. Oxford, UK: Clarendon Press.
3. Bird E. 2008 *Coastal geomorphology: an introduction*, 2nd edn. Chichester, UK: John Wiley & Sons.
4. Bezore R, Kennedy DM, Ierodiaconou D. 2016 The drowned apostles: the longevity of sea stacks over eustatic cycles. *J. Coast. Eng.* **75**, 592–596.
5. Wakeman WF. 1891 *A hand-book of Irish antiquities, pagan and Christian; especially of such as are of easy access from the Irish metropolis*. Dublin, Ireland: Hodges, Figgis, and Co.
6. Best JL, Wignall PB (eds). 2016 *Field guide to the carboniferous sediments of the Shannon Basin, Western Ireland*. Chichester, UK: John Wiley and sons.
7. Trenhaile AS. 2002 Rock coasts, with particular emphasis on shore platforms. *Geomorphology* **48**, 7–22. (doi:10.1016/S0169-555X(02)00173-3)
8. Trenhaile AS, Pepper DA, Trenhaile RW, Dalimonte M. 1998 Stacks and notches at Hopewell Rocks, New Brunswick, Canada. *Earth Surf. Process. Landf.* **23**, 975–988. (doi:10.1002/(SICI)1096-9837(1998110)23:11<975::AID-ESP916>3.0.CO;2-K)
9. Shepard FP, Kuhn GG. 1983 History of sea arches and remnant stacks of La Jolla, California, and their bearing on similar features elsewhere. *Mar. Geol.* **51**, 139–161. (doi:10.1016/0025-3227(83)90094-4)
10. Fannon JS, Fowler AC, Moyles IR. 2017 Numerical simulations of drumlin formation. *Proc. R. Soc. Lond. A* **473**, 20170220. (doi:10.1098/rspa.2017.0220)
11. Seminara G. 2006 Meanders. *J. Fluid Mech.* **554**, 271–297. (doi:10.1017/S0022112006008925)
12. Schwämmle V, Herrmann H. 2004 Modelling transverse dunes. *Earth Surf. Process. Landf.* **29**, 769–784. (doi:10.1002/esp.1068)
13. Fowler AC, Mayer C. 2017 The formation of ice sails. *Geophys. Astrophys. Fluid Dyn.* **111**, 411–428. (doi:10.1080/03091929.2017.1370092)
14. Dyson JL. 1952 Ice-ridged moraines and their relation to glaciers. *Am. J. Sci.* **250**, 204–211. (doi:10.2475/ajs.250.3.204)
15. Hoppe G, Schytt V. 1953 Some observations on fluted moraine surfaces. *Geografisker Ann.* **35**, 105–115. (doi:10.1080/20014422.1953.11880852)
16. Boulton GS. 1976 The origin of glacially-fluted surfaces: observations and theory. *J. Glaciol.* **17**, 287–309. (doi:10.3189/S0022143000013605)
17. Gordon JE, Whalley WB, Gellatly AF, Vere DM. 1992 The formation of glacial flutes: assessment of models with evidence from Lyngsdalen, North Norway. *Quat. Sci. Rev.* **11**, 709–731. (doi:10.1016/0277-3791(92)90079-N)
18. Naylor LA, Stephenson WJ, Trenhaile AS. 2010 Rock coast geomorphology: recent advances and future research directions. *Geomorphology* **114**, 3–11. (doi:10.1016/j.geomorph.2009.02.004)
19. Trenhaile A. 2016 Rocky coasts—their role as depositional environments. *Earth-Sci. Rev.* **159**, 1–13. (doi:10.1016/j.earscirev.2016.05.001)
20. Trenhaile AS. 2019 Hard-rock coastal modelling: past practice and future prospects in a changing world. *J. Marine Sci. Eng.* **7**, 34. (doi:10.3390/jmse7020034)
21. Arróspide C, Aguilar G, Martinod J, Rodriguez MP, Regard V. 2023 Coastal cliff evolution: modelling the long-term interplay between marine erosion, initial topography, and uplift in an arid environment. *Geomorphology* **428**, 108642. (doi:10.1016/j.geomorph.2023.108642)

22. Matsumoto H, Dickson ME, Kench PS. 2016 An exploratory numerical model of rocky shore profile evolution. *Geomorphology* **268**, 98–109. (doi:10.1016/j.geomorph.2016.05.017)
23. Palermo RV, Perron JT, Soderblom JM, Birch SPD, Hayes AG, Ashton AD. 2024 NEWTS1.0: numerical model of coastal erosion by waves and transgressive scarps. *Geosci. Model Dev.* **17**, 3433–3445. (doi:10.5194/gmd-17-3433-2024)
24. Robinet A, Idier D, Castelle B, Marieu V. 2018 A reduced-complexity shoreline change model combining longshore and cross- shore processes: the LX-Shore model. *Environ. Modell. Softw.* **109**, 1–16. (doi:10.1016/j.envsoft.2018.08.010)
25. Valvo LM, Murray AB, Ashton A. 2006 How does underlying geology affect coastline change? An initial modeling investigation. *J. Geophys. Res.* **111**, F02025. (doi:10.1029/2005JF000340)
26. Ashton AD, Walkden MJA, Dickson ME. 2011 Equilibrium responses of cliffed coasts to changes in the rate of sea level rise. *Marine Geol.* **284**, 217–229. (doi:10.1016/j.margeo.2011.01.007)
27. Ashton A, Murray AB, Arnoult O. 2001 Formation of coastline features by large-scale instabilities induced by high-angle waves. *Nature* **414**, 296–300. (doi:10.1038/35104541)
28. Ashton AD, Murray AB. 2006 High-angle wave instability and emergent shoreline shapes: 1. Modeling of sand waves, flying spits, and capes. *J. Geophys. Res. Earth Surf.* **111**, F04011.
29. Limber PW, Murray AB. 2011 Beach and sea cliff dynamics as a driver of rocky coastline evolution and stability. *Geology* **39**, 1149–1152. (doi:10.1130/G32315.1)
30. Limber PW, Murray AB. 2014 Unraveling the dynamics that scale cross-shore headland relief on rocky coastlines: 2. Model predictions and initial tests. *J. Geophys. Res. Earh Surf.* **119**, 874–891. (doi:10.1002/2013JF002978)
31. Limber PW, Murray AB, Adams PN, Goldstein EB. 2014 Unraveling the dynamics that scale cross-shore headland relief on rocky coastlines: 1. Model development. *J. Geophys. Res. Earth Surf.* **119**, 854–873. (doi:10.1002/2013JF002950)
32. López-Fernández C, Domínguez-Cuesta MJ, González-Pumariega P, Ballesteros D, Suárez LS, Jiménez-Sánchez M. 2022 Instability mechanisms and evolution of a rocky cliff on the Atlantic coast of Spain. *J. Coast. Conserv.* **26**, 60. (doi:10.1007/s11852-022-00907-x)
33. Kroy K, Sauermann G, Herrmann HJ. 2002 Minimal model for aeolian sand dunes. *Phys. Rev. E* **66**, 031302. (doi:10.1103/PhysRevE.66.031302)
34. Ikeda S, Parker G, Sawai K. 1981 Bend theory of river meanders. Part 1. Linear development. *J. Fluid Mech.* **112**, 363–377. (doi:10.1017/S0022112081000451)
35. Lee EM. 2008 Coastal cliff behavior: observations on the relationship between beach levels and recession rates. *Geomorphology* **101**, 558–571. (doi:10.1016/j.geomorph.2008.02.010)
36. Sunamura T. 1982 A wave tank experiment on the erosional mechanism at a cliff base. *Earth Surf. Process. Landf.* **7**, 333–343. (doi:10.1002/esp.3290070405)
37. Sunamura T. 1976 Feedback relationship in wave erosion of laboratory rocky coast. *J. Geol.* **84**, 427–437. (doi:10.1086/628209)
38. Komar PD. 1971 The mechanics of sand transport on beaches. *J. Geophys. Res.* **76**, 713–721. (doi:10.1029/JC076i003p00713)
39. Komar PD. 1976 *Beach processes and sedimentation*. Englewood Cliffs, NJ: Prentice-Hall.
40. Limber PW, Murray AB. 2015 Sea stack formation and the role of abrasion on beach-mantled headlands. *Earth Surf. Process. Landf.* **40**, 559–568. (doi:10.1002/esp.3667)
41. Kline SW, Adams PN, Limber PW. 2014 The unsteady nature of sea cliff retreat due to mechanical abrasion, failure and communication feedbacks. *Geomorphology* **219**, 53–67. (doi:10.1016/j.geomorph.2014.03.037)
42. Longuet-Higgins MS. 1970 On the longshore currents generated by obliquely incident sea waves, 1. *J. Geophys. Res.* **75**, 6778–6789. (doi:10.1029/JC075i033p06778)
43. Meyer-Peter E, Müller R. 1948 Formulas for bed-load transport. In *Proc. Int. Assoc. Hydraul. Res., 3rd Annual Conf., Stockholm*, pp. 39–64.
44. Shields A. 1936 Anwendung der Ähnlichkeits mechanik und der Turbulenzforschung auf die Geschiebebewegung. Mitteilung der Preussischen Versuchanstalt für Wasserbau und Schiffbau, Heft 26, Berlin.
45. Fowler AC, Kopteva N, Oakley C. 2007 The formation of river channels. *SIAM J. Appl. Math.* **67**, 1016–1040. (doi:10.1137/050629264)
46. Ashton AD, Murray AB. 2006 High-angle wave instability and emergent shoreline shapes: 2. Wave climate analysis and comparisons to nature. *J. Geophys. Res.* **111**, F04012.
47. Bowen AJ. 1969 The generation of longshore currents on a plane beach. *J. Mar. Res.* **27**, 206–215.

48. Sunamura T. 2015 Rocky coast processes: with special reference to the recession of soft rock cliffs. *Proc. Jpn Acad. B* **91**, 481–500. (doi:10.2183/pjab.91.481)
49. Murray JD. 2002 *Mathematical biology*, 2 volumes. Berlin, Germany: Springer–Verlag.
50. Anand SK, Bertagni MB, Singh A, Porporato A. 2023 Eikonal equation reproduces natural landscapes with threshold hillslopes. *Geophys. Res. Lett.* **50**, GL105710. (doi:10.1029/2023GL105710)
51. Fowler A, McGuinness M. 2019 *Chaos: an introduction for applied mathematicians*. Switzerland: Springer Nature.
52. Howard LN, Kopell N. 1977 Slowly varying waves and shock structures in reaction-diffusion equations. *Stud. Appl. Math.* **56**, 95–145. (doi:10.1002/sapm197756295)
53. Grindrod P. 1991 *Patterns and waves: the theory and applications of reaction-diffusion equations*. Oxford: Oxford University Press.
54. Chapman SJ, Lawry JMH, Ockendon JR, Tew RH. 1999 On the theory of complex rays. *SIAM Rev.* **41**, 417–509. (doi:10.1137/S0036144599352058)
55. Flemings MC. 1974 *Solidification processing*. New York: McGraw-Hill.
56. Smith TR, Bretherton FP. 1972 Stability and the conservation of mass in drainage basin evolution. *Water Resour. Res.* **8**, 1506–1529. (doi:10.1029/WR008i006p01506)
57. Gómez-Pazo A, Pérez-Alberti A, Trenhaile A. 2021 Tracking clast mobility using RFID sensors on a boulder beach in Galicia, NW Spain. *Geomorphology* **373**, 107514. (doi:10.1016/j.geomorph.2020.107514)
58. Shadrick JR, Rood DH, Hurst MD, Piggott MD, Hebditch BG, Seal AJ, Wilcken KM. 2022 Sea-level rise will likely accelerate rock coast cliff retreat rates. *Nature Commun.* **13**, 7005. (doi:10.1038/s41467-022-34386-3)
59. Regard V, Prémaillon M, Dewez TJB, Carretier S, Jeandel C, Godderis Y, Bonnet S, Schott J, Pedoja K, Martinod J, Viers J, Fabre S. 2022 Rock coast erosion: an overlooked source of sediments to the ocean. Europe as an example. *Earth Planet. Sci. Lett.* **579**, 117356. (doi:10.1016/j.epsl.2021.117356)
60. Gómez-Pazo A, Pérez-Alberti A, Trenhaile A. 2021 Tracking the behavior of rocky coastal cliffs in northwestern Spain. *Environ. Earth Sci.* **80**, 757. (doi:10.1007/s12665-021-09929-4)
61. Felton EA. 2002 Sedimentology of rocky shorelines: 1. A review of the problem, with analytical methods, and insights gained from the Hulopoe Gravel and the modern rocky shoreline of Lanai, Hawaii. *Sed. Geol.* **152**, 221–245. (doi:10.1016/S0037-0738(02)00070-2)
62. Fowler AC, Kember GC, Ng FSL. 2025 Towards a theory for the formation of sea stacks. Figshare. (doi:10.6084/m9.figshare.c.8116001)